RESEARCH ARTICLE | DECEMBER 15 2023

A planar cloverleaf antenna for circularly polarized microwave fields in atomic and molecular physics experiments

Weijun Yuan ; Siwei Zhang ; Niccolò Bigagli ; Claire Warner ; Ian Stevenson ; Sebastian Will

Rev. Sci. Instrum. 94, 123201 (2023)
https://doi.org/10.1063/5.0167572
CHORUS

Review of Scientific Instruments ARTICLE pubs.aip.org/aip/rsi

A planar cloverleaf antenna for circularly polarized microwave fields in atomic and molecular physics experiments

Cite as: Rev. Sci. Instrum. 94, 123201 (2023); doi: 10.1063/5.0167572
Submitted: 13 July 2023 • Accepted: 19 November 2023 •
Published Online: 15 December 2023

Weijun Yuan,[a] Siwei Zhang, Niccolò Bigagli, Claire Warner, Ian Stevenson, and Sebastian Will[a]

AFFILIATIONS

Department of Physics, Columbia University, New York, New York 10027, USA

[a]Authors to whom correspondence should be addressed: wy2336@columbia.edu and sebastian.will@columbia.edu

ABSTRACT

We report on the design and characterization of a compact microwave antenna for atomic and molecular physics experiments. The antenna is comprised of four loop antennas arranged in a cloverleaf shape, allowing for precise adjustment of polarization by tuning the relative phase of the loops. We optimize the antenna for left-circularly polarized microwaves at 3.5 GHz and characterize its near-field performance using ultracold NaCs molecules as a precise quantum sensor. Observing an unusually high Rabi frequency of $2\pi \times 46.1(2)$ MHz, we extract an electric field amplitude of 33(2) V/cm at 22 mm distance from the antenna. The polarization ellipticity is $2.3(4)^\circ$, corresponding to a 24 dB suppression of right-circular polarization. The cloverleaf antenna is planar and provides large optical access, making it highly suitable for quantum control of atoms and molecules and potentially other quantum systems that operate in the microwave regime.

I. INTRODUCTION

Microwave fields play a key role in modern technology. In everyday life, numerous applications rely on the emission and detection of microwaves, from microwave ovens to wireless data communication.[1–3] In quantum science, the active use of microwaves dates back to the 1930s, when, for the first time, a nuclear spin was flipped by applying an oscillating microwave field.[4] Recently, the importance of microwave fields in quantum science has rapidly risen. Many high-quality qubit platforms operate in the microwave regime,[5] including superconducting qubits,[6] nitrogen-vacancy (NV) centers,[7] quantum dots,[8] trapped ions,[9–11] neutral atoms,[12,13] and dipolar molecules.[14] The precise control of microwave wavelength, power, and polarization is of paramount importance to generate quantum superposition and entangled states with high fidelity.

In particular, the generation of microwaves with well-controlled polarization becomes increasingly important. Clean polarization ensures coupling between a well-defined pair of quantum states. While the generation of pure linear polarization is relatively straightforward, the creation of clean circularly polarized microwave fields is more challenging. The latter has been critical for the recent demonstration of microwave shielding of ultracold dipolar molecules by our group and others,[15–20] which has motivated the design of the antenna presented in this work. Circularly polarized microwaves also play a critical role in the preparation of circular atomic Rydberg states,[21] which are expected to find applications as long-lived qubits,[22–24] and in the control of hyperfine qubits in alkali atoms, for example for microwave clock operation,[25] or to realize mid-circuit measurement protocols in advanced quantum algorithms.[26] Beyond atoms and molecules, we expect that antenna technologies to produce clean circularly polarized microwaves can also find applications in other quantum systems and qubit platforms.

Fundamentally, there are two approaches to create circularly polarized microwave fields: Designs based on a helical antenna naturally produce circular polarization as a result of the helix geometry.[27–29] The handedness of the polarization is determined by the helicity of the antenna and cannot be tuned *in situ*. In addition, helical antennas often require a reflector,[30] which is not easy to tune and can hinder optical access. Alternatively, circular polarization arises by superimposing two linearly polarized microwave fields

with an appropriate phase difference. This can be achieved using two orthogonal modes of a rectangular waveguide,[31] two microwave horns,[26] or antenna arrays with a discrete rotational symmetry.[32] Typical antenna designs are often bulky, and integration into quantum science setups, which have limited space and other constraints, can be challenging.

In this article, we describe the design and characterization of a microwave antenna array that consists of four loop antennas arranged in a cloverleaf shape. The array is planar and features large optical access, and the microwave polarization can be flexibly tuned by adjusting the relative phases between the loops. Here, we optimize the array for left-circular polarization[33] in the near field and characterize its properties by driving a rotational transition of sodium–cesium (NaCs) molecules, positioned 22 mm away from the antenna. We observe a strong microwave coupling with a Rabi frequency of $2\pi \times 46.1(2)$ MHz, corresponding to an electric field of 33(2) V/cm. In addition, we measure a high purity of circular polarization with an ellipticity of 2.3(4)°.

II. DESIGN

Our antenna array is designed for an operating frequency of 3.47 GHz, corresponding to an in-vacuum wavelength of 86.5 mm. In the design, we particularly focus on the near-field operation, which corresponds to working distances from the antenna that are smaller than the emission wavelength. The array consists of four elliptical loop antennas that are arranged in a cloverleaf shape, as shown in Fig. 1. All loops are oriented in the same direction such that the array has a fourfold rotational symmetry. Each loop has a semi-major axis of 16.7 mm and a semi-minor axis of 10 mm. The circumference is 86.5 mm. A 3D-printed mount made of PETG plastic holds the four loops in place [see Fig. 1(b)]. A hole with a diameter of 20 mm allows for laser beams to propagate through the middle. The antenna array is less than 1 mm thick.

The individual loop antennas are made of 75 Ω coax BNC cables, following Ref. 34 [see Fig. 1(a)]. The jacket and the inner insulator are peeled off to expose the inner copper wire on a length that is slightly longer than one wavelength in vacuum. The copper wire is bent into an elliptical shape, and its end is soldered to the braided metal shield of the coax cable to form a loop. The impedance of the resulting one-wavelength antenna in the array has a real part of 100 Ω with an additional imaginary contribution. To impedance match it to the 50 Ω microwave system, we employ a quarter-wavelength transformer and stub-tuning. The quarter-wavelength transformer changes the real part of the antenna impedance to 50 Ω; it is implemented by leaving the length of the unstripped part between the loop antenna and the BNC connector to be 5/4 of the wavelength in the 75 Ω BNC cable. An open circuit tuning stub cancels the imaginary part of the impedance; using a T-adaptor, it is inserted between the 75 Ω cable and the 50 Ω cable that comes from the microwave amplifiers [see Fig. 1(d)]. This setup suppresses the reflections from the antenna by about 10 dB. We measure a bandwidth of 40 MHz for a single loop antenna.

Each loop generates a linearly polarized microwave field oscillating along its semi-major axis [see Fig. 1(a)]. By combining the loops in different ways, the polarization of the array can be flexibly tuned. The pair A–C (B–D) generates a microwave field that is

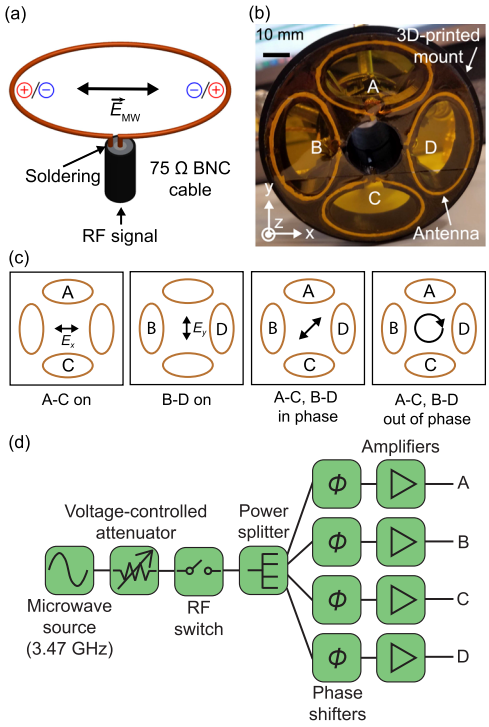

FIG. 1. Planar cloverleaf microwave antenna. (a) Drawing of a single loop. (b) Picture of the antenna array. A 3D-printed structure (black) serves as a mount. Each loop is wrapped in white Teflon tape for insulation. The bottom of the antenna mount is covered by Kapton tape to protect the viewport of the vacuum chamber that the antenna is mounted on. (c) Tunability of the microwave polarization of the array. When pair A–C (B–D) is active, the electric field E_x (E_y) is linearly polarized along the horizontal (vertical) axis. When A–C and B–D are operated in phase (out of phase), 45° linear polarization (circular polarization) is generated. (d) Electronic setup supplying the cloverleaf antenna.

linearly polarized along the x (y)axis, which we denote by E_x (E_y) [see Fig. 1(c)]. To maximize E_x (E_y), we set the phase difference between loops A and C (B and D) to π. The polarization of the entire antenna array is controlled by the phase difference between E_x and E_y. In order to create left (right)-circularly polarized microwave fields, we set the phase difference of E_x relative to E_y to be $-\pi/2$ ($+\pi/2$). In this work, we have optimized the antenna for left-circular polarization to maximize coupling to a σ^+-rotational transition of NaCs molecules (see Sec. IV).

The electronics stack supplying the cloverleaf antenna is shown in Fig. 1(d). A microwave generator (Rohde & Schwarz SMA100B) produces a 3.47 GHz sine wave, whose amplitude can be tuned by a voltage-controlled attenuator (General Microwave D1954-OPT62) and switched by a RF switch (Mini-Circuits ZYSWA-2-50DR+). The signal is then split into four branches with a power splitter (Mini-Circuits ZN4PD1-63-S+). To tune the phases, we change the effective cable length between the power splitter and the amplifiers by inserting a series of commercial SMA adapters, which act as passive phase shifters. Then, each signal is amplified by a 15 W amplifier

(Mini-Circuits ZHL-15W-422X-S+) and connected to one of the loop antennas.

III. NUMERICAL SIMULATION

We numerically simulate the performance of the cloverleaf antenna, mostly focusing on the near-field operation. Using the Antenna Toolbox in MATLAB,[35] we calculate the radiation pattern. For comparison, we also consider a helical antenna.[30] Helical antennas naturally produce circularly polarized microwaves when operating in axial mode. They have widely been used in atomic and molecular physics experiments,[18,36–39] making them a good standard for comparison. The parameters of the helical antenna are chosen to balance the electric field amplitude and polarization purity. We assume a helix with ten turns and a pitch spacing of 15 mm. The radius of the helix is 13.8 mm and the radius of the reflector disk is 32.4 mm, as shown in Fig. 2(a).

As shown in Fig. 2(b), for a given total input power, the cloverleaf antenna has a stronger electric field amplitude than the helical antenna. At a specific distance of $z_0 = 22$ mm, relevant for the antenna characterization in Sec. IV, it is 1.6 times larger. This comes also with a larger electric field gradient for the cloverleaf antenna in the near field. Figure 2(c) shows the radial amplitude profile for z_0. Compared with the helical antenna, the electric field amplitude of the cloverleaf array shows a stronger curvature in the radial direction.

In addition, the directivity in the far field of the two designs shows a marked difference. In the axial direction (90°), it is 6.2 dBi for the cloverleaf and 13.4 dBi for the helical antenna, indicating a higher directivity of the helical antenna. Given the symmetry of its design, the cloverleaf antenna emits symmetrically in the forward and backward directions. The electric field amplitude in the far field falls off quickly, and the near-field operation is favored. In addition, we calculate the reflection coefficient (S_{11} parameters) for different microwave frequencies to quantify reflections from the antenna, including the stub tuning.[40] The calculation yields a voltage standing wave ratio (VSWR) 2:1 bandwidth of 80 MHz, which is compatible with the measured bandwidth of a single loop.

IV. EXPERIMENTAL CHARACTERIZATION

We experimentally characterize the cloverleaf antenna in terms of electric field amplitude and purity of left-circular polarization. To this end, we employ ultracold NaCs ground state molecules as an extremely sensitive quantum sensor. The antenna is mounted directly on the glass viewport of a stainless-steel vacuum chamber, 22 mm away from the molecular sample, surrounded by copper coils that are used to generate homogeneous magnetic fields, as illustrated in Fig. 3(a). The details on the preparation and quantum-state resolved detection of NaCs ground state molecules are reported in earlier work from our group.[41–44] In short, NaCs molecules are prepared in the vibrational and rotational ground states, $|J, m_J\rangle = |0,0\rangle$, where J is the rotational quantum number and m_J is its projection on the quantization axis, which is defined by a magnetic field of 864 G along the vertical direction. From $|0,0\rangle$, three excited rotational states, $|1,-1\rangle$, $|1,0\rangle$, and $|1,+1\rangle$, can be accessed via an electric dipole transition at a frequency of 3.47 GHz. The left-circularly polarized microwave fields drive the σ^+-transition to $|1,+1\rangle$.

First, we measure the amplitude of the electric microwave field. To this end, we measure the Rabi frequency Ω of the microwave drive, which is related to the electric field amplitude via $E = \hbar\Omega/d_{\mathrm{tr}}$, where d_{tr} is the transition dipole moment. To record the data shown in Fig. 3(b), we switch on a resonant microwave field, let the molecules evolve under the microwave field for a variable time, switch the field off, and measure the population in state $|0,0\rangle$. We observe unusually fast Rabi oscillations between states $|0,0\rangle$ and $|1,+1\rangle$ with a Rabi frequency $\Omega/(2\pi) = 46.1(2)$ MHz, indicating a strong microwave electric field. The transition dipole for the σ^+-transition is given by $d_{\mathrm{tr}} = d_{\mathrm{NaCs}}/\sqrt{3}$, where $d_{\mathrm{NaCs}} = 4.75(20)$ D is the permanent electric dipole moment of the NaCs molecules.[45] From this, we extract an electric field amplitude of 33(2) V/cm at distance z_0.

Second, we characterize the purity of left-circular polarization. In the microwave frame, the polarization purity can be quantified by the ellipticity, defined by $\xi = \arctan(E'_-/E'_+)$, where E'_-/E'_+ is the ratio of the electric field amplitude proportional to the ratio of Rabi frequencies of the $\sigma^\pm$-transitions in the microwave frame. In the lab

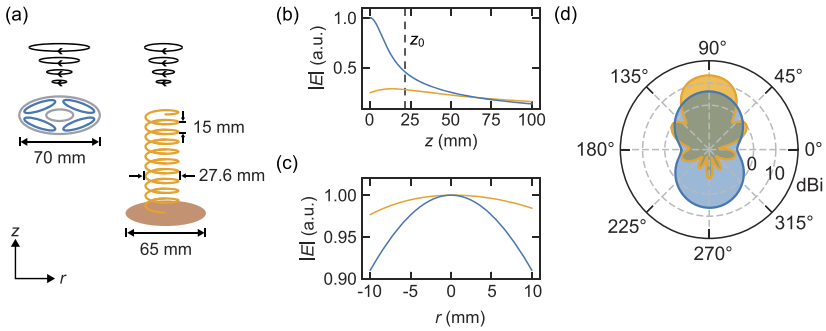

FIG. 2. Simulation of the cloverleaf array and a reference helical antenna. Data in blue (orange) refer to the cloverleaf (helical) antenna. (a) Geometry of the antenna array and the helical antenna used in the simulation. (b) Amplitude of the total electric field along the axial direction. z is measured from the top of the antenna for both designs. The vertical dashed line indicates $z_0 = 22$ mm, the distance where the antenna is experimentally used and characterized in Sec. IV. (c) Total electric field amplitude in the radial direction for z_0. The electric field amplitude is normalized to the value at position $r = 0$ mm for both antennas. (d) Calculated directivity of both designs. The axial z-direction corresponds to 90° in this plot.

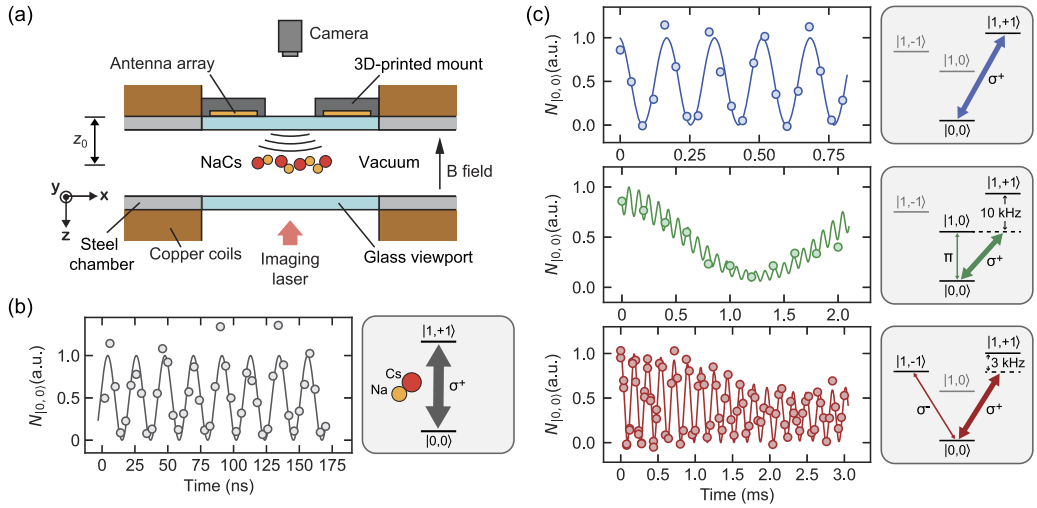

FIG. 3. Characterization of the cloverleaf antenna with ultracold NaCs molecules. (a) The antenna array sits on top of a fused silica viewport of an ultrahigh vacuum chamber. The distance between the antenna and the molecules is $z_0 = 22$ mm or 0.26λ, where λ is the wavelength of the resonant microwave field. (b) Fast Rabi oscillations on the σ^+-transition. The solid line is a sinusoidal fit. (c) Slow Rabi oscillations on the σ^+- (upper panel), $\pi-$ (middle panel), and σ^--transitions (lower panel) at low microwave power. The blue solid line is a sinusoidal fit to extract Ω_+. To extract Ω_π, a three-level model is employed to account for off-resonant coupling on the σ^+-transition manifested as fast jitter on top of the slow oscillation. The green solid line shows the three-level fit. For the σ^--transition, a beat envelope is observed due to the interference between the resonant σ^--transition and the off-resonant σ^+-transition. The red solid line shows the three-level fit.

frame, since the propagation direction of the microwave is not perfectly aligned with the quantization axis defined by the magnetic field, we not only measure $\sigma^\pm$-coupling to $|1,+1\rangle$ and $|1,-1\rangle$, respectively, but also measure π-coupling to $|1,0\rangle$. From the measured data, a coordinate transform to the microwave frame yields the ratio E'_-/E'_+. To achieve a high spectral resolution, the measurements are performed with low microwave intensity.

We measure resonant Rabi oscillations between $|0,0\rangle$ and $|1,+1\rangle$ with $\Omega_+ = 2\pi\times$ 5.8(4) kHz, as shown in the upper panel of Fig. 3(c). To obtain Ω_π, we tune the microwave frequency on resonance with the $|0,0\rangle$ to $|1,0\rangle$ transition, as shown in the middle panel of Fig. 3(c). Fitting the data with a three-level model, which takes into account off-resonant σ^+-coupling, we obtain $\Omega_\pi = 2\pi \times 0.38(7)$ kHz. Finally, we extract Ω_- by tuning the microwave frequency on resonance with the $|0,0\rangle$ to $|1,-1\rangle$ transition, as shown in the lower panel of Fig. 3(c). As the energy splitting between $|1,+1\rangle$ and $|1,-1\rangle$ is only 3 kHz, the σ^+ and σ^- transitions are simultaneously driven, giving rise to the beat envelope in the data. We fit the data with a three-level model and obtain $\Omega_- = 2\pi\times$ 0.23(2) kHz. From the ratio of Rabi frequencies, we calculate the ratio of electric field amplitudes $E_-/E_+ = 0.040(6)$ and $E_\pi/E_+ = 0.066(13)$ in the lab frame. As the phase relations between the electric field components cannot be measured directly, we cannot exactly determine the tilt angle between the propagation direction of the microwaves and the magnetic field. By sampling all possible phases, we determine that the tilt angle lies in the range of 5.1(7)°–5.5(7)°.[46] From this, we infer the ratio of E'_-/E'_+ and obtain the ellipticity ranging from 2.1(2)° to 2.4(2)°, corresponding to 2.3(4)°.

V. DISCUSSION

Key features of the cloverleaf antenna are the compact form factor, the relatively high electric field amplitude in the near field, and the flexible tunability of the output polarization without the need to make physical changes to the antenna itself. This is especially useful for the correction of imperfections, such as reflections and field distortions from boundary conditions in the implementation environment. By tuning the relative phase between the loops, it is possible to switch the antenna from σ^+ to σ^- polarization on demand. This degree of freedom is absent in helical antennas, where the polarization is set by the helicity of the spiral. We have demonstrated a small ellipticity in a challenging experimental environment with stainless steel and copper structures in the direct vicinity. In free space, likely even smaller ellipticity can be achieved. In this work, we have optimized the ellipticity for the electric field, as the system was used to drive an electric dipole transition. It is worth noting that the polarization purity can also be optimized for magnetic fields as relevant for magnetic dipole transitions.[47] It should also be possible to adapt the design of the antenna, which is implemented here for a resonance frequency of 3.47 GHz, for microwave frequencies in a range from 1 to 20 GHz by adjusting the circumference of the individual loop antennas within practical limits.

It should be possible to further improve the performance of the cloverleaf antenna with straightforward modifications. The electric field amplitudes produced by each elliptical loop likely differ by a small amount due to cross-coupling between the loops, asymmetric reflections from the surrounding metal parts, imperfect manufacturing, or minor differences in the electronics stack of each loop. By

adding amplitude control on the input of each elliptical loop, such inhomogeneities can be compensated and even finer control over the polarization purity could be achieved. Furthermore, it should be possible to increase the directivity of the cloverleaf antenna by adding a reflector that reflects the backward radiation into the forward direction. Our simulations show that this can increase the electric field amplitude by a factor of 1.6. In addition, the inclusion of dynamical phase shifters in the electronics stack could further enhance the flexibility of the design. Finally, the form factor and thickness can be further reduced by implementing the antenna as a printed circuit board (PCB). This may also allow for the direct integration into different experimental platforms, including setups in cryogenic environments, reaching beyond the use in atomic and molecular setups.

VI. CONCLUSION

We have presented a cloverleaf microwave antenna array with a high electric field amplitude and a high polarization purity. It features a simple design, compact form factor, ease of manufacturing, and flexible fine-tuning of polarization. In recent work, we have successfully used the antenna to realize collisionally stable NaCs ground state molecules, which enabled the first evaporative cooling of ultracold bosonic molecules.[19] More generally, we expect our antenna design to facilitate the control of molecular rotational states, which are expected to find applications in quantum simulation[48] and quantum computing,[49,50] thanks to long intrinsic coherence times.[51] In addition, the cloverleaf antenna may be useful for the implementation of quantum computing schemes with circular Rydberg atoms that require a low ellipticity $\xi < 2.5^\circ$ to achieve high fidelity,[24] which we have shown here to be within reach. In addition, our design should be broadly adaptable for microwave quantum state control of atoms, from evaporative cooling of magnetically trapped atoms to the manipulation of atomic hyperfine qubits,[52,53] as well as other quantum systems that require precise microwave control.

ACKNOWLEDGEMENTS

This work was supported by an NSF CAREER Award (Award No. 1848466), an ONR DURIP Award (Award No. N00014-21-1-2721), and a Lenfest Junior Faculty Development Grant from Columbia University. C.W. acknowledges the support from the Natural Sciences and Engineering Research Council of Canada (NSERC). W.Y. acknowledges the support from the Croucher Foundation. I.S. was supported by the Ernest Kempton Adams Fund. S.W. acknowledges the additional support from the Alfred P. Sloan Foundation.

AUTHOR DECLARATIONS

Conflict of Interest

The authors have no conflicts to disclose.

Author Contributions

W.Y. and S.Z. contributed equally to this work.

Weijun Yuan: Conceptualization (equal); Investigation (equal); Writing – original draft (equal); Writing – review & editing (equal). **Siwei Zhang**: Conceptualization (equal); Investigation (equal); Writing – original draft (equal); Writing – review & editing (equal). **Niccolò Bigagli**: Investigation (equal). **Claire Warner**: Investigation (equal). **Ian Stevenson**: Conceptualization (equal); Investigation (equal); Writing – original draft (equal); Writing – review & editing (equal). **Sebastian Will**: Conceptualization (equal); Investigation (equal); Supervision (equal); Writing – original draft (equal); Writing – review & editing (equal).

DATA AVAILABILITY

The data that support the findings of this study are available from the corresponding author upon reasonable request.

REFERENCES

[1] T. K. Ishii, *Handbook of Microwave Technology* (Elsevier, 1995).
[2] T. Ohlsson and N. Bengtsson, *Microwave Technology and Foods* (Elsevier, 2001).
[3] M. Golio and J. Golio, *RF and Microwave Applications and Systems* (CRC Press, 2018).
[4] I. I. Rabi, Phys. Rev. **51**, 652 (1937).
[5] J. C. Bardin, D. H. Slichter, and D. J. Reilly, IEEE J. Microw. **1**, 403 (2021).
[6] A. Blais, R.-S. Huang, A. Wallraff, S. M. Girvin, and R. J. Schoelkopf, Phys. Rev. A **69**, 062320 (2004).
[7] D. D. Awschalom, R. Hanson, J. Wrachtrup, and B. B. Zhou, Nat. Photonics **12**, 516 (2018).
[8] B. E. Kane, Nature **393**, 133 (1998).
[9] H. Häffner, C. F. Roos, and R. Blatt, Phys. Rep. **469**, 155 (2008).
[10] C. Ospelkaus, U. Warring, Y. Colombe, K. Brown, J. Amini, D. Leibfried, and D. J. Wineland, Nature **476**, 181 (2011).
[11] D. Aude Craik, N. Linke, T. Harty, C. Ballance, D. Lucas, A. Steane, and D. Allcock, Appl. Phys. B **114**, 3 (2014).
[12] A. D. Ludlow, M. M. Boyd, J. Ye, E. Peik, and P. O. Schmidt, Rev. Mod. Phys. **87**, 637 (2015).
[13] L. Henriet, L. Beguin, A. Signoles, T. Lahaye, A. Browaeys, G.-O. Reymond, and C. Jurczak, Quantum **4**, 327 (2020).
[14] L. D. Carr, D. DeMille, R. V. Krems, and J. Ye, New J. Phys. **11**, 055049 (2009).
[15] T. Karman and J. M. Hutson, Phys. Rev. Lett. **121**, 163401 (2018).
[16] T. Karman and J. M. Hutson, Phys. Rev. A **100**, 052704 (2019).
[17] L. Anderegg, S. Burchesky, Y. Bao, S. S. Yu, T. Karman, E. Chae, K.-K. Ni, W. Ketterle, and J. M. Doyle, Science **373**, 779 (2021).
[18] A. Schindewolf, R. Bause, X.-Y. Chen, M. Duda, T. Karman, I. Bloch, and X.-Y. Luo, Nature **607**, 677 (2022).
[19] N. Bigagli, C. Warner, W. Yuan, S. Zhang, I. Stevenson, T. Karman, and S. Will, Nat. Phys. **19**, 1579–1584 (2023).
[20] J. Lin, G. Chen, M. Jin, Z. Shi, F. Deng, W. Zhang, G. Quéméner, T. Shi, S. Yi, and D. Wang, Phys. Rev. X **13**, 031032 (2023).
[21] J.-M. Raimond, M. Brune, and S. Haroche, Rev. Mod. Phys. **73**, 565 (2001).
[22] A. Facon, E.-K. Dietsche, D. Grosso, S. Haroche, J.-M. Raimond, M. Brune, and S. Gleyzes, Nature **535**, 262 (2016).
[23] T. L. Nguyen, J.-M. Raimond, C. Sayrin, R. Cortinas, T. Cantat-Moltrecht, F. Assemat, I. Dotsenko, S. Gleyzes, S. Haroche, G. Roux *et al.*, Phys. Rev. X **8**, 011032 (2018).
[24] S. R. Cohen and J. D. Thompson, PRX Quantum **2**, 030322 (2021).
[25] S. Bize, P. Laurent, M. Abgrall, H. Marion, I. Maksimovic, L. Cacciapuoti, J. Grünert, C. Vian, F. P. d. Santos, P. Rosenbusch *et al.*, J. Phys. B: At., Mol. Opt. Phys. **38**, S449 (2005).

[26]T. Graham, L. Phuttitarn, R. Chinnarasu, Y. Song, C. Poole, K. Jooya, J. Scott, A. Scott, P. Eichler, and M. Saffman, "Midcircuit measurements on a single-species neutral alkali atom quantum processor," Phys. Rev. X (to be published 2023).
[27]J. D. Kraus, Proc. IRE **37**, 263 (1949).
[28]U. R. Kraft, IEEE Trans. Antennas Propag. **44**, 515 (1996).
[29]J. D. Kraus and R. J. Marhefka, *Antennas for All Applications*, 3rd ed. (McGraw-Hill, 2021).
[30]C. A. Balanis, *Antenna Theory: Analysis and Design* (John Wiley & Sons, 2015).
[31]X.-Y. Chen, A. Schindewolf, S. Eppelt, R. Bause, M. Duda, S. Biswas, T. Karman, T. Hilker, I. Bloch, and X.-Y. Luo, Nature **614**, 59 (2023).
[32]A. Signoles, "Manipulations cohérentes d'états de Rydberg elliptiques par dynamique Zénon quantique," Ph.D. thesis, Université Pierre et Marie Curie-Paris VI, 2014.
[33]The handedness is defined as left-handed (right-handed) if the electric field is rotating counterclockwise (clockwise) observed from the point of view of the source.
[34]D. E. Miller, "Studying coherence in ultra-cold atomic gases," Ph.D. thesis, Massachusetts Institute of Technology, 2007.
[35]The Antenna Toolbox in MATLAB employs the method of moments (MoM) and the results are crosschecked by running simulations on COMSOL, which uses the finite element method (FEM).
[36]A. Öttl, S. Ritter, M. Köhl, and T. Esslinger, Rev. Sci. Instrum. **77**, 063118 (2006).
[37]M. Boguslawski, "All-microwave control of hyperfine states in ultracold spin-1 rubidium," Ph.D. thesis, Georgia Institute of Technology, 2019.
[38]Y.-G. Zheng, L. Jiang, Z.-H. Zhu, W.-Y. Zhang, Z.-Y. Zhou, B. Xiao, and Z.-S. Yuan, Rev. Sci. Instrum. **93**, 064701 (2022).
[39]S. Borówka, U. Pylypenko, M. Mazelanik, and M. Parniak, "Continuous wideband microwave-to-optical converter based on room-temperature Rydberg atoms," Nat. Photonics (published online 2023).
[40]S. W. Ellingson, *Electromagnetics*, 2 (Virginia Tech Publishing, 2020).
[41]C. Warner, A. Z. Lam, N. Bigagli, H. C. Liu, I. Stevenson, and S. Will, Phys. Rev. A **104**, 033302 (2021).
[42]A. Z. Lam, N. Bigagli, C. Warner, W. Yuan, S. Zhang, E. Tiemann, I. Stevenson, and S. Will, Phys. Rev. Res. **4**, L022019 (2022).
[43]I. Stevenson, A. Z. Lam, N. Bigagli, C. Warner, W. Yuan, S. Zhang, and S. Will, Phys. Rev. Lett. **130**, 113002 (2023).
[44]C. Warner, N. Bigagli, A. Z. Lam, W. Yuan, S. Zhang, I. Stevenson, and S. Will, New J. Phys. **25**, 053036 (2023).
[45]P. J. Dagdigian and L. Wharton, J. Chem. Phys. **57**, 1487 (1972).
[46]For a given phase relation between the electric field components, we determine the Euler angles of the rotational transformation from the lab frame to the microwave frame by requiring the electric field component along the propagation direction of the microwave (or the linear π-polarization component) to be zero in the microwave frame. Then we rotate the electric field components to the microwave frame with this set of Euler angles and calculate the ratio E'_-/E'_+ to extract the ellipticity. We scan the phase relations and obtain the range of tilt angles and the corresponding ellipticity. This procedure has been used and described in Ref. 18.
[47]We have experimentally confirmed this by driving the $|F = 1, m_F = 1\rangle$ to $|F = 2, m_F = 2\rangle$ hyperfine transition of Na atoms at large magnetic field, such that the energy spacing is approximately 3.5 GHz. Here F is the total angular momentum and m_F its projection on the axis of the magnetic field. This is a σ^+ magnetic dipole transition. We have found that we can reach a Rabi frequency of about $2\pi \times 100$ kHz and a polarization purity that corresponds to an ellipticity of about 4°.
[48]J. L. Bohn, A. M. Rey, and J. Ye, Science **357**, 1002 (2017).
[49]D. DeMille, Phys. Rev. Lett. **88**, 067901 (2002).
[50]R. Krems, B. Friedrich, and W. C. Stwalley, *Cold Molecules: Theory, Experiment, Applications* (CRC Press, 2009).
[51]P. D. Gregory, L. M. Fernley, A. L. Tao, S. L. Bromley, J. Stepp, Z. Zhang, S. Kotochigova, K. R. Hazzard, and S. L. Cornish, arXiv:2306.02991 (2023).
[52]D. Bluvstein, H. Levine, G. Semeghini, T. T. Wang, S. Ebadi, M. Kalinowski, A. Keesling, N. Maskara, H. Pichler, M. Greiner *et al.*, Nature **604**, 451 (2022).
[53]T. Graham, Y. Song, J. Scott, C. Poole, L. Phuttitarn, K. Jooya, P. Eichler, X. Jiang, A. Marra, B. Grinkemeyer *et al.*, Nature **604**, 457 (2022).